Chalcogenide Letters Vol. 21, No. 2, February 2024, p. 189 - 200

Study of electronic structure, elastic and thermodynamic properties of Cu_2MgSnS_4 under different pressures

H. J. Hou[a,*], Su Fan[a], H. Y. Wang[a], W. X. Chen[a], X. W. Lu[a], S. R. Zhang[b], L. H. Xie[c]

[a]*School of Materials Engineering, Yancheng Institute of Technology, Yancheng, 224051, China*

[b]*School of Physics, Electronics and Intelligent Manufacturing, Huaihua University, Huaihua, 418008, China*

[c]*School of Physics and Electronic Engineering, Sichuan Normal University, Chengdu, 610066, China*

The electronic structure, elastic and thermodynamic properties of Cu_2MgSnS_4 was studied based on density functional theory (DFT). The results show that Cu_2MgSnS_4 is a direct bandgap semiconductor. The B/G of Cu_2MgSnS_4 is greater than 1.75, indicating that Cu_2MgSnS_4 is a ductile material. Through the study of thermodynamic properties, it is found that the temperature increases, the bulk modulus B and Debye temperature Θ decrease, while the heat capacity C_V, entropy S, Grüneisen constant γ and thermal expansion coefficient α increase, and the heat capacity is close to the Dulong-Petit limit. As the pressure increases, the bulk modulus B, Debye temperature Θ increases, while the entropy S, Grüneisen constant γ and heat capacity C_V decrease.

(Received December 5, 2023; Accepted February 20, 2024)

Keywords: Cu_2MgSnS_4, Electronic structure, Elastic properties, Thermodynamic properties

1. Introduction

In recent years, quaternary chalcogenides (I_2-II-IV-VI_4) have attracted the attention of scientists for their flexibility and functionality, making them promising in thermoelectric, nonlinear optics and photovoltaic technologies [1-2]. The development of Cu_2MgSnS_4 is list of semiconductor materials, which has complex structure and various properties. Therefore, many researches are focused on Cu_2MgSnS_4. The Cu_2MgSnS_4 has been synthesized by hot injection methods, where it was found that Cu_2MgSnS_4 crystallizes in the kesterite (KS) structure [3]. The powder of $Cu_2MgSnSe_4$ was synthesized by solid state reaction in a disordered sample of the ST structure [4]. Bekki have studied the structural, electronic, optical, and elastic properties of Cu_2MgSnS_4 in four crystalline phases (wurtzite-stannite (WS), stannite (ST), kesterite (KS), and primitive-mixed CuAu (PMCA)) using density functional theory [5]. In 2018, Bekki et al also carried out theoretical studies on the heat capacity, thermal expansion coefficient and Debye temperatures of Cu_2MgSnX_4 (X = S, Se and Te) quaternary compounds [6]. Although some

* Corresponding author: wyezhhj@126.com
https://doi.org/10.15251/CL.2024.212.189

theoretical calculation methods and experimental have been used to study the properties of Cu_2MgSnS_4, there are still some deficiencies. Little attention has been paid to the elastic constants and thermodynamic properties at high temperatures and pressures, which are important to extend our knowledge to the performance of Cu_2MgSnS_4. Therefore, it is necessary to study the effect of temperature and pressure on Cu_2MgSnS_4.

2. Computational methods

In this paper, the first-principles method based on the plane wave pseudopotential is used to calculate the crystal structure and elastic properties of Cu_2MgSnS_4 with the using of the CASTEP package [7]. In the calculation, the exchange correlation potential is calculated by the generalized gradient approximation (GGA) of Perdew-Burke-Ernzerhof (PBE)[8], and the vanderbilt ultrasoft pseudopotential [9] is used with the cutoff energy of 450 eV for the considered structure. The *k* point meshes of 4×4×4 for Cu_2MgSnS_4 is generated using the Monkhorst-Pack scheme.

3. Results and discussion

3.1. Structural properties

Cu_2MgSnS_4 is a tetragonal semiconductor of type I_2-II-IV-VI_4. The lattice constants of Cu_2MgSnS_4 are $a = b = 5.6882$Å, $c = 11.3378$ Å. The coordinates of Cu, Mg, Sn and S were (0, 0.5, 0.25), (0, 0 , 0), (0, 0, 0.5), (0.2587, 0.2587, 0.3714), respectively. The electronic structure, elastic and thermodynamic properties of Cu_2MgSnS_4 was studied. The crystal structure is shown in Fig. 1.

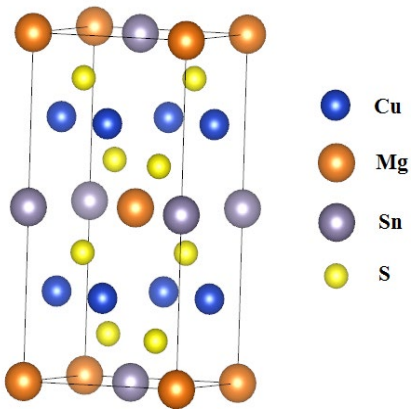

Fig.1. The crystal structure of Cu_2MgSnS_4.

In the calculation process, we used LDA and GGA approximation methods to optimize the Cu_2MgSnS_4 and compared the data based on the lattice constants of Cu_2MgSnS_4. The results are shown in Table 1.

Table 1. The optimized lattice constants of Cu_2MgSnS_4 *by different methods.*

	LDA	GGA-PBE	GGA-RPBE	GGA-PW91	GGA-WC	Theo.[6]	Exp.[10]
a = *b* (Å)	5.4313	5.4729	5.6361	5.4603	5.5179	5.783	5.568
c(Å)	10.5803	10.6928	11.0506	10.6783	10.7819	11.3578	10.932

From the data in the table above, we can see that compared with the experimental values, the minimum relative error of lattice constants *a* and *c* is obtained by using the generalized gradient approximation (GGA) exchange correlation potential for RPBE, where the error between *a* and *b* and experimental values is 0.9%, the error between *c* and the experimental value is 2.5%, while the largest relative error is calculated using local-density approximation (LDA). Because the relative error between the results calculated by GGA-RPBE method and the experimental values is the least, that is, more close to the experimental values, it shows that the results obtained by this method are very reliable, so we use RPBE-GGA method in the following calculation.

3.2. Band structure

After optimizing Cu_2MgSnS_4 at zero pressure, the GGA-RPBE method can be used to calculate band structure (as shown in Fig. 2) and density of state (DOS) (as shown in Fig. 3). From Fig. 3, we can see that neither the bottom line of the conduction band nor the top line of the valence band passes through the Fermi level, which means that Cu_2MgSnS_4 is a direct bandgap semiconductor with a bandgap of 0.291 eV. The total densities of states and the partial densities of states of Cu_2MgSnS_4 is shown in Fig. 3. As can be seen from Fig. 3, the band of Cu_2MgSnS_4 consists of two parts, in which the lower band of Cu_2MgSnS_4 is mainly contributed by the p orbital of Mg, which varies from -45 eV to -40 eV. When the energy band of Cu_2MgSnS_4 varies from -13.89 eV to 11.28 eV, the p orbitals of S and Sn, the s orbitals of Mg and the d orbitals of Cu cross. The valence electron structure of Cu atom is: $3d^{10}4s^1$, the valence electron structure of Mg atom is: $3s^2$, the valence electron structure of Sn atom is: $5s^25p^2$, the valence electron structure of S atom is: $3s^23p^4$. The valence band width at the top of Cu_2MgSnS_4 is about -2.183 eV ~ -0.017 eV, and there is a peak at -1.61 eV. The main contribution of this peak is from the d orbital of Cu atom. The width of the middle valence band is about -13.94 eV ~ -2.38 eV, and there are four peaks at -12.76 eV, -7.58 eV, -5.08 eV, -3.51 eV. The peak at -12.76 eV is mainly contributed by the p-orbital of S. The peak positions at -7.58 eV are contributed by the s orbitals of Sn, and the peak positions at -5.08 eV and -3.51 eV are contributed by the d orbitals of S, the lowest band width is about -42.95 eV ~ -41.73 eV, and it has a peak at -42.40 eV, which is contributed by the Mg p orbital.

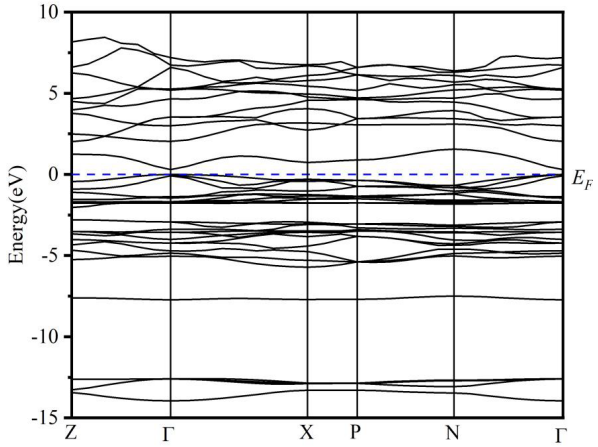

Fig. 2 Calculated energy band structure of Cu_2MgSnS_4 at zero pressure.

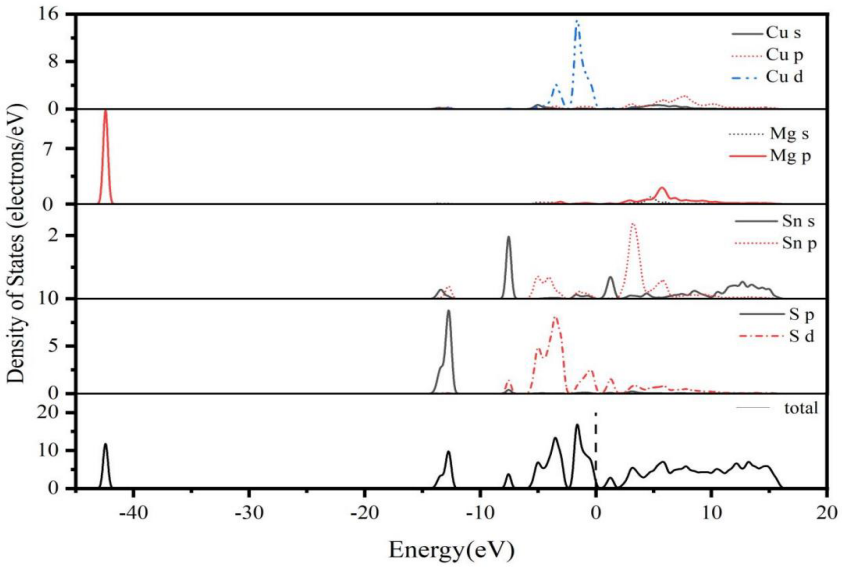

Fig. 3. Calculated the partial density of states and the density of states of Cu_2MgSnS_4 at zero pressure.

3.3. Mechanical properties

The number of independent elastic constants for chalcopyrite structure is six (C_{11}, C_{12}, C_{13}, C_{33}, C_{44} and C_{66}). Elastic stiffness tensor components must satisfy certain relations known as Born stability criteria [11], which for the tetragonal chalcopyrite requires that

$$C_{11}, C_{33}, C_{44}, C_{66}>0,\ \ C_{11} > \left|C_{12}\right|, C_{11}C_{33} > C_{13}^2, \text{ and } \ (C_{11}+C_{12})C_{33} > 2C_{13}^2 \qquad (1)$$

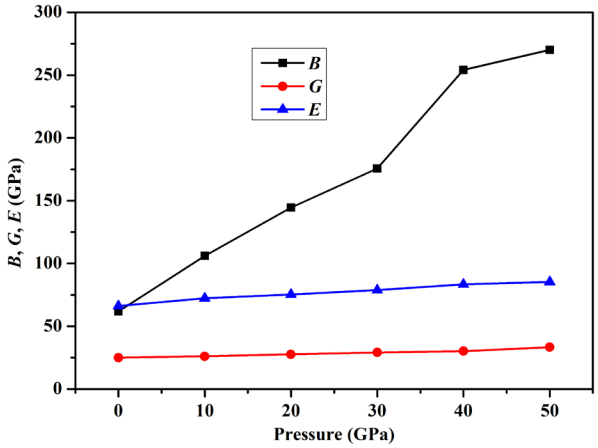

Fig. 4. The calculated elastic constants (C_{ij}) of Cu_2MgSnS_4 at select pressures.

From Fig. 4, we can see that the four independent elastic constants of Cu_2MgSnS_4, C_{11}, C_{33}, C_{12}, and C_{13}, increase with increasing pressure from 0 to 50 GPa, the growth rate of C_{33} in the range of 30-40 GPa is smaller than that in the range of 0-30 GPa. While C_{44} and C_{66} increased in the range of 0-10 GPa, but slowly decreased in the later 10-50 GPa, and overall, the changes of C_{44} and C_{66} were not as large as those of C_{11}, C_{33}, C_{12}, and C_{13}, this shows that the two independent elastic constants are far less sensitive to pressure than the other four independent elastic constants, and the elastic constants satisfy the conditions of mechanical stability, in other words, the crystal structure of Cu_2MgSnS_4 is mechanically stable. The calculated elastic constants agree with other theoretical values [5], which shows the correctness of our calculation.

Table 2. Calculated elastic constants C_{ij} (GPa), bulk modulus B(GPa), shear modulus G (GPa), Young's modulus E (GPa) of Cu_2MgSnS_4 at different pressures.

Pressure	C_{11}	C_{33}	C_{44}	C_{66}	C_{12}	C_{13}	B	G	E	B/G
0	85.03	68.92	37.74	42.27	55.85	52.64	61.75	25	66.11	2.47
0 Theo.[5]	95.2	93.196	32.616	39.723	66.066	62.494	73.932	25.121	67.695	2.940
10	124.31	117.24	42.96	46.95	101.84	96.81	106.09	26.09	72.36	4.06
20	154.73	158.16	19.84	36.92	143.72	136.65	144.61	27.63	75.26	5.23
30	176.44	187.13	12.43	24.53	172.98	170.81	175.68	29.17	78.82	6.02
40	222.67	213.22	10.18	15.52	210.33	210.28	254.14	30.23	83.29	8.41
50	243.77	275.29	14.49	17.25	235.78	234.58	270.13	33.34	85.29	8.10

Then, when the Cu_2MgSnS_4 is in the range of 0-50 GPa, according to the elastic constants at different pressures, Voigt-Reuss-Hill approximation [12-14] was used to calculate the bulk modulus B, shear modulus G, Young's modulus E and B/G of Cu_2MgSnS_4. The above parameters are shown in Table 2. According to the Voigt-Reuss-Hill approximation, the formulas for calculating the bulk modulus B, shear modulus G and Young's modulus E are:

$$B_V = \frac{1}{9}(2C_{11} + C_{33} + 2C_{12} + 4C_{13}) \tag{2}$$

$$B_R = \frac{(C_{11} + C_{12})C_{33} - 2C_{13}^2}{C_{11} + C_{12} + 2C_{33} - 4C_{13}} \tag{3}$$

$$G_V = \frac{1}{15}(2C_{11} + C_{33} - C_{12} - 2C_{13} + 6C_{44} + 3C_{66}) \tag{4}$$

$$G_R = 15\left\{18B_V / C^2 + 6/(C_{11} - C_{12}) + 6/C_{44} + 3/C_{66}\right\}^{-1} \tag{5}$$

Here

$$C^2 = (C_{11} + C_{12})C_{33} - 2C_{13}^2 \tag{6}$$

$$B = \frac{1}{2}(B_V + B_R) \tag{7}$$

$$G = \frac{1}{2}(G_V + G_R) \tag{8}$$

$$E = 9BG/(3B + G) \tag{9}$$

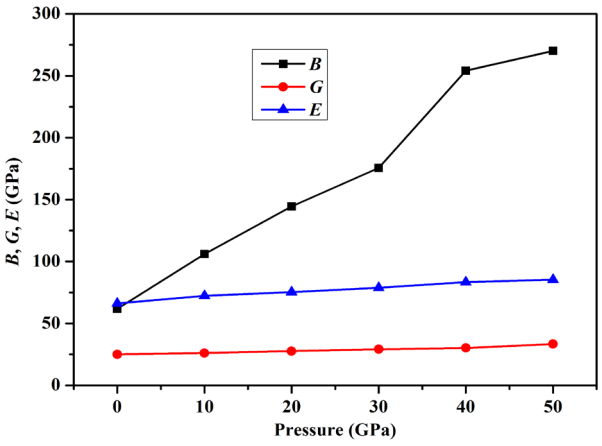

Fig. 5. Bulk modulus B, shear modulus G, Young's modulus E of Cu_2MgSnS_4 at select pressures.

From Fig. 5, we can see that *B*, *G* and *E* all increase with the pressure, but the increase of *B* is much larger than that of the other two. According to the Pugh standard, whether a solid material is ductile or brittle depends on the *B*/*G* ratio. If *B*/*G* < 1.75, the material is brittle. When *B*/*G* >1.75[15] , it is a ductile material. From Table 2, we can know that Cu_2MgSnS_4 is a ductile material.

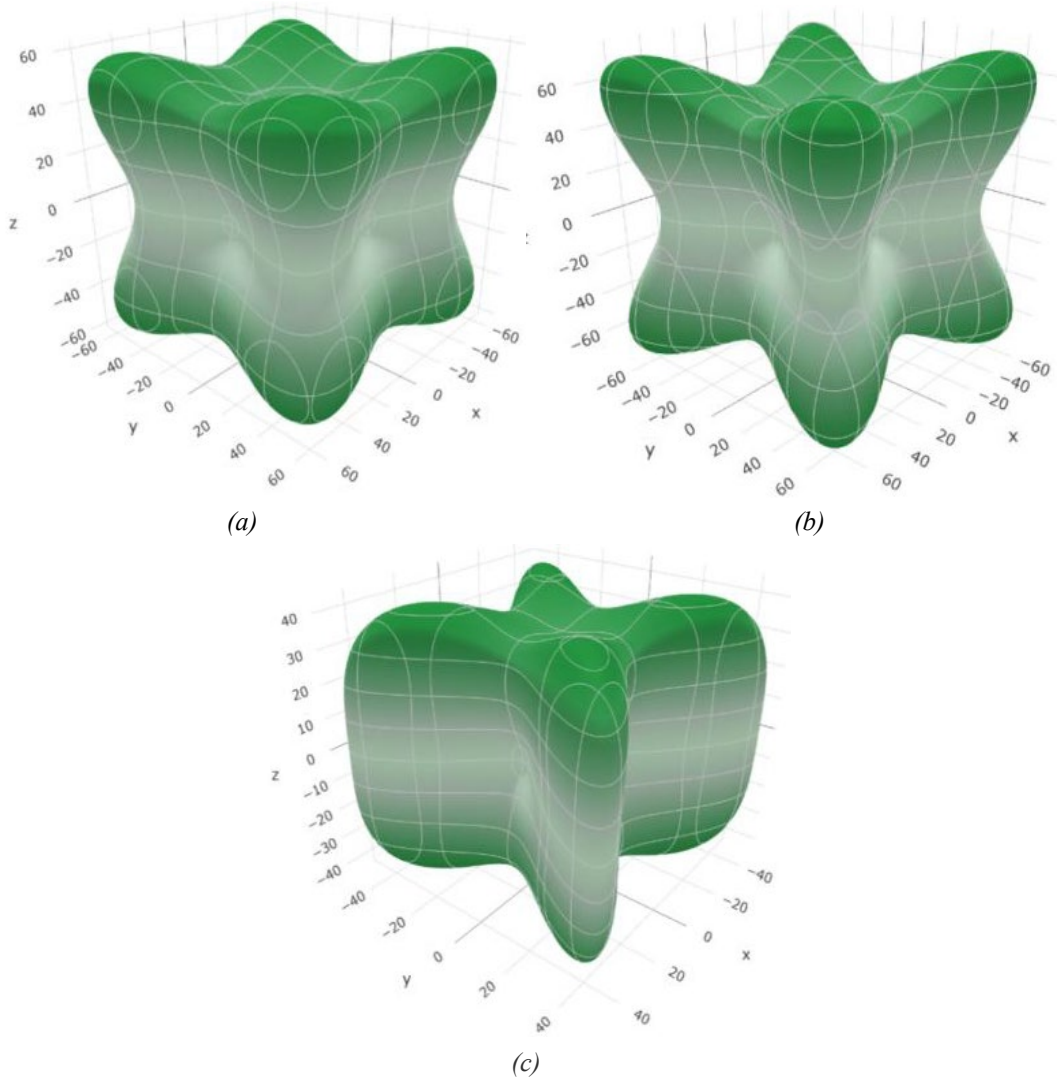

Fig. 6. The surface contours of Young's modulus of Cu_2MgSnS_4 (a): 0 GPa, (b): 30 GPa, (c): 50 GPa).

In order to understand the anisotropic properties of Cu_2MgSnS_4, the three-dimensional (3D) surfaces with Young's modulus *E* is constructed [16]. From Fig. 6, we can see that Cu_2MgSnS_4 shows anisotropy at 0GPa, 30GPa, and 50GPa, and the degree of variation increases with increasing pressure.

3.3. Thermodynamic properties

Based on the quasi-harmonic Debye model [17], we calculated thermodynamic parameters of Cu_2MgSnS_4 at different temperatures and pressures. Fig. 7 shows the relationship between bulk modulus and pressure at different temperatures. It can be seen that the bulk modulus of Cu_2MgSnS_4 increases rapidly with the increase of pressure. Combined with Fig. 7 and 8, we can see that the bulk modulus at low temperature is higher than that at high temperature under any pressure.

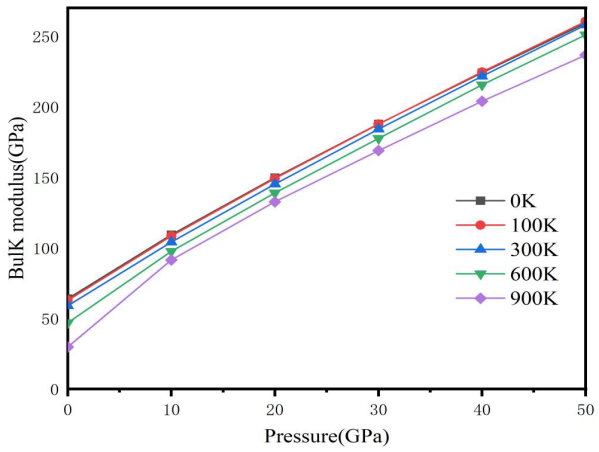

Fig. 7. The relationship between B and P of Cu_2MgSnS_4 at different temperatures.

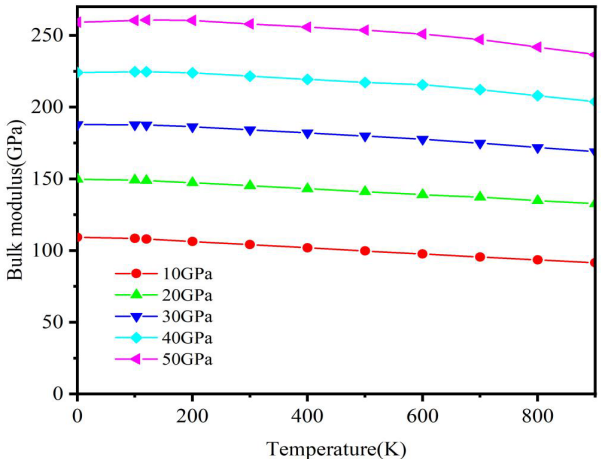

Fig. 8. The relationship between B and T of Cu_2MgSnS_4 at different pressures.

Fig. 9 shows the relationship between heat capacity C_V and temperature at different pressures. At the same pressure, the heat capacity C_V increases with the increase of temperature. It can be seen from the figure that at 0-350 K, the increase of heat capacity C_V is much greater than that at 350 K-900 K, and with the increase of temperature, it eventually converges to the Dulong-Petit limit. From Fig. 10, we can find that the C_V and C_P curves tend to be consistent below 200 K, but C_P still tends to increase at 0 GPa when the temperature is above 200 K.

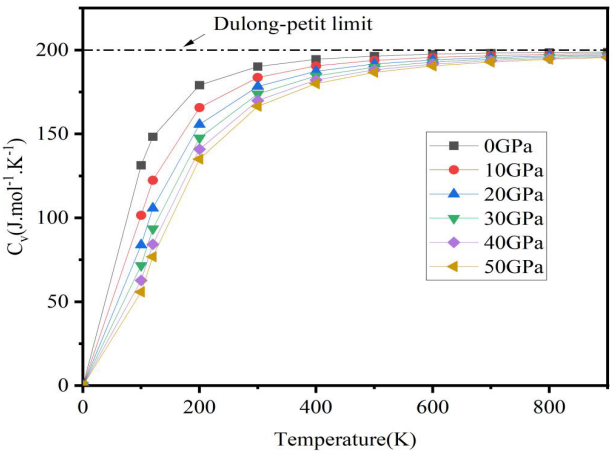

Fig. 9. The relationship between C_V and T of Cu_2MgSnS_4 under different pressures.

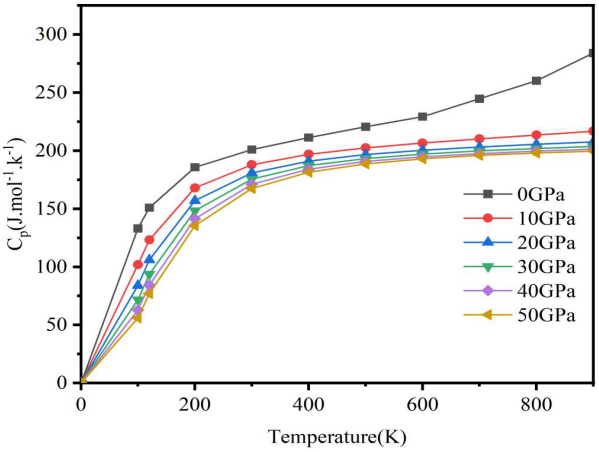

Fig. 10. The relationship between C_P and T of Cu_2MgSnS_4 under different pressures.

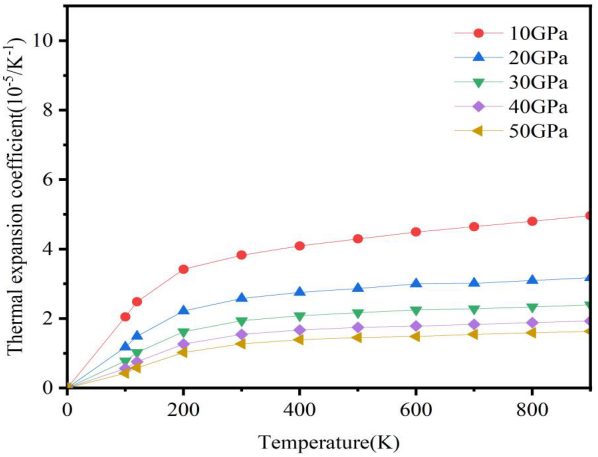

Fig. 11. The relationship between thermal expansion coefficient and temperature of Cu_2MgSnS_4 at different pressures.

Fig. 11 shows the relationship between thermal expansion coefficient and temperature at different pressures. As we can see from the Fig. 11, the thermal expansion coefficient increases rapidly when the temperature is below 200 K, and decreases as the pressure increases. With the increase of temperature, the thermal expansion coefficient curve tends to flatten gradually at 20-50GPa, especially when the temperature is above 800K, the thermal expansion coefficient hardly changes any more. But the thermal expansion coefficient α at 10 GPa is still slightly increasing above 800K.

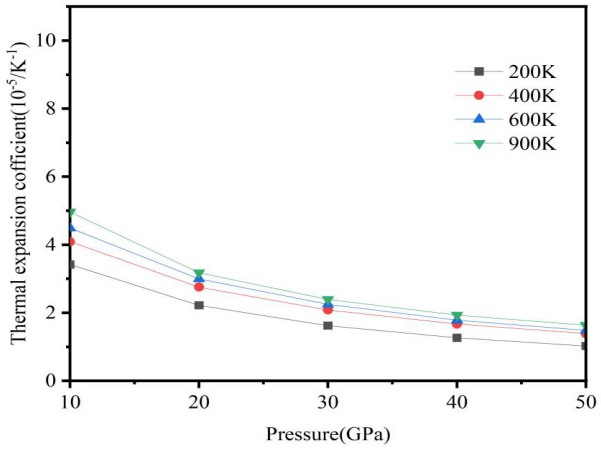

Fig. 12. The relationship between thermal expansion coefficient and pressure of Cu_2MgSnS_4 at different temperatures.

From Fig.12, we can see that the thermal expansion coefficient α at 200K, 400K, 600K, and 900K decrease rapidly as the pressure increases from 10 GPa to 20 GPa. However, as the pressure increased from 20 GPa to 50 GPa, the thermal expansion coefficient α decreased more slowly. At pressures above 30 GPa, thermal expansion coefficient α values at 600 K and 900 K are very close, which means that at high temperatures and pressures, temperature and pressure have little effect on thermal expansion coefficient α.

Table 3. Calculated entropy S, Debye temperature Θ and Grüneisen constant γ of Cu_2MgSnS_4 at different temperatures and pressures.

T/K	*P*/GPa	0	10	20	30	40	50
100	*S*	84.356	52.979	39.329	31.402	26.242	22.587
	Θ	302.94	396.30	459.22	508.59	549.25	584.22
	γ	2.512	2.017	1.790	1.640	1.526	1.431
300	*S*	272.764	221.616	193.673	175.177	161.686	151.172
	Θ	297.17	390.59	455.77	506.24	547.58	582.90
	γ	2.554	2.040	1.801	1.647	1.531	1.435
600	*S*	424.641	359.127	326.760	305.387	289.303	277.336
	Θ	272.43	380.13	448.82	501.25	545.01	580.24
	γ	2.757	2.085	1.824	1.661	1.538	1.488
900	*S*	296.372	444.883	409.365	386.486	369.188	356.051
	Θ	241.02	368.88	441.54	495.95	541.64	579.24
	γ	3.091	2.136	1.849	1.677	1.547	1.445

Table 3 shows our calculated entropy, Debye temperature and Grüneisen constant for Cu_2MgSnS_4 at different temperatures and pressures. At present, no relevant thermodynamic data can be used as reference, and we hope that our data can provide theoretical help for experimental authors.

4. Conclusions

The band structure, density of states, elastic properties and thermodynamic properties of Cu_2MgSnS_4 is calculated by first-principles calculation. The calculated results show that Cu_2MgSnS_4 crystal is a direct band gap semiconductor with a bandgap of 0.291 eV. The elastic constants, bulk modulus, shear modulus, Young's modulus and B/G of Cu_2MgSnS_4 is calculated. It is found that the $B/G > 1.75$ of Cu_2MgSnS_4, so we can know that Cu_2MgSnS_4 is a ductile material. Finally, we studied the thermodynamic properties of Cu_2MgSnS_4. We calculated the bulk modulus B, heat capacity C_V, C_P, thermal expansion coefficient α of Cu_2MgSnS_4 at temperatures ranging from 0 to 50 GPa and from 0 to 900 K.

References

[1] X.Y. Shi, F.Q. Huang, M.L. Liu, L.D. Chen, Appl. Phys. Lett. 94 (2009) 122103; https://doi.org/10.1063/1.3103604.

[2] Q.Guo, G. M.Ford, W. C.Yang, B. C.Walker, E. A. Stach, H. W. Hillhouse, R. Agrawal, J. Am. Chem. Soc. 132 (2010) 17384 https://doi.org/10.1021/ja108427b

[3] V. Pavan Kumar, E. Guilmeau, B. Raveau, V. Caignaert, U.V. Varadaraju, J. Appl. Phys. 118 (15) (2015) 155101; https://doi.org/10.1063/1.4933277.

[4] M. Wei, Q. Du, R. Wang, G. Jiang, W. Liu, C. Zhu, Chem. Lett. 43 (2014) 1149; https://doi.org/10.1246/cl.140208.

[5] B. Bekki, K. Amara, M. El Keurti, Chin. Phys. B 26(2017) 076201; https://doi.org/10.1088/1674-1056/26/7/076201

[6] B. Bekki, K. Amara, N. Marbouh, F. Khelfaoui, Y. Benallou, M. Elkeurti, A. Bentaye, Comput. Condens. Matte. 16 (2018) e00339; https://doi.org/10.1016/j.cocom.2018.e00339

[7] S. J. Clark, M. D. Segall, C. J. Pickard, Z. Kristallogr 220(2005) 567; https://doi.org/10.1524/zkri.220.5.567.65075

[8] J.P. Perdew, K. Burke, M. Ernzerhof , Phys. Rev. Lett.77(1996)3865; https://doi: 10.1103/PhysRevLett.77.3865

[9] D. Vanderbilt, Phys. Rev. B 41(1990)7892 https://doi.org/10.1103/PhysRevB.41.7892

[10] G. H. Zhong, K. F. Tse, Y. O. Zhang, X. G. Li, L. Huang, C. L. Yang, J. Y. Zhu, Z. Zeng, Z.Y. Zhang, X. D. Xiao, Thin Solid Films 603 (2016)224; https://doi.org/10.1016/j.tsf.2016.02.005

[11] M. Born, K. Huang, Dynamical Theory of Crystal Lattices (Oxford: Clarendon) 1954.

[12] W. Voigt Lehrbuchder Kristallphysik Teubner Leipzig (1928)

[13] A. Reuss, Z. Angew. Math. Mech. 9, 49 (1929); https://doi.org/10.1002/zamm.19290090104

[14] R. Hill, Proc. Phys. Soc. 65(1952) 349; https://doi.org/10.1088/0370-1298/65/5/307

[15] S. F. Pugh, Philos. Mag. 45, 823 (1954); https://doi.org/10.1080/14786440808520496

[16] R. Gaillac, P. Pullumbi, F.-X. Coudert,J. Phys. Condens. Matter 28, 275201(2016); https://doI.org/10.1088/0953-8984/28/27/275201

[17] M. A. Blanco, A. Martín Pendás, E. Francisco, J. M. Recio, R.Franco, J. Mol. Struc-Theochem. 368, 245(1996); https://doi.org/10.1016/S0166-1280(96)90571-0